Stokes flows in a 2D bifurcation

Yidan Xue[1], Stephen J. Payne[2], Sarah L. Waters[1]

[1]Mathematical Institute, University of Oxford, UK.
[2]Institute of Applied Mechanics, National Taiwan University, Taiwan.

E-mail(s): xue@maths.ox.ac.uk; stephenpayne@ntu.edu.tw;
waters@maths.ox.ac.uk;

Abstract

The flow network model is an established approach to approximate pressure-flow relationships in a network, which has been widely used in many contexts. However, little is known about the impact of bifurcation geometry on such approximations, so the existing models mostly rely on unidirectional flow assumption and Poiseuille's law, and thus neglect the flow details at each bifurcation. In this work, we address these limitations by computing Stokes flows in a 2D bifurcation using LARS (Lightning-AAA Rational Stokes), a novel mesh-free algorithm for solving 2D Stokes flow problems utilising an applied complex analysis approach based on rational approximation of the Goursat functions. Using our 2D bifurcation model, we show that the fluxes in two child branches depend on not only pressures and widths of inlet and outlet branches, as most previous studies have assumed, but also detailed bifurcation geometries (e.g. bifurcation angle), which were not considered in previous studies. The 2D Stokes flow simulations allow us to represent the relationship between pressures and fluxes of a bifurcation using an updated flow network, which considers the bifurcation geometry and can be easily incorporated into previous flow network approaches. The errors in the flow conductance of a channel in a bifurcation approximated using Poiseuille's law can be greater than 16%, when the centreline length is twice the inlet channel width and the bifurcation geometry is highly asymmetric. In addition, we present details of 2D Stokes flow features, such as flow separation in a bifurcation and flows around fixed objects at different locations, which previous flow network models cannot capture. These findings suggest the importance of incorporating detailed flow modelling techniques alongside existing flow network approaches when solving complex flow problems.

Keywords: Stokes flow, flow network, bifurcation, lightning solver, biharmonic equation

1

1 Introduction

The computation of fluid flows within networks plays a significant role in addressing many engineering challenges. For instance, quantifying the blood flows in an organ or an organ system can help us better understand their physiological functions [10]. Models for network flow can also provide valuable insights into vascular diseases [24] to improve their treatments [19].

The standard way to compute flows in a network is via a flow network modelling approach, which is a 0D reduced-order modelling of the underlying 3D fluids problem, where junctions and boundary points of the network are represented by nodes with flow segments between them. By assuming steady unidirectional flow with no-slip wall conditions in each flow segment, the flow conductance in each segment is described by Poiseuille's law [32]:

$$G = \frac{q}{\Delta p} = \frac{\pi d^4}{128 \mu l} = \frac{1}{R},\tag{1}$$

where q is the flow rate, Δp is the pressure drop across the segment, d is the diameter, μ is the viscosity, l is the segment length, and R is the flow resistance, which is the inverse of conductance and also commonly used. After prescribing the pressures at boundary nodes of the network and imposing continuity of fluxes at each internal nodes, a linear system between pressures and fluxes in the network can be constructed [31], if the viscosity is a constant or a function of diameter only. From this "pressure-flux relationship", the fluxes can be solved easily using a standard linear solver when pressures are known or vice versa. Note that the pressure-flux relationship is no longer linear when the viscosity depends on other factors, e.g. the volume of red blood cells when considering blood flow [25, 28, 29], then a non-linear solver will be needed.

The flow network approach has been widely used for microvascular flows [29], with applications to oxygen transport [13, 30] and drug delivery [8]. In addition, the flow network model has been used to compute flows in microfluidic devices for biomedical applications [17, 23]. These applications rely on the ability of the flow network model to provide a good approximation for Stokes flows in a complex network. However, the assumption of unidirectional flow no longer hold precisely at the junction region, causing errors in predicting the pressure-flow relationship and the flow partition at the junction. Such errors can build up when considering large networks with a large number of junctions. Furthermore, as a 0D approach, the flow network model neglects the flow details at the bifurcation, making it impossible to investigate fluid-structure interaction problems, e.g. the microparticle partition at a bifurcation [1].

To the best of our knowledge, Stokes flows in a bifurcation have not yet been thoroughly studied either analytically or numerically, even for a 2D setup. Analytical or semi-analytical solutions exist for simpler 2D Stokes flow problems including flows near a corner [20], in a partitioned channel [14], in an expanded channel [16] or a constricted channel [33]. However, these analytical techniques are not suitable for solving 2D Stokes flows in an bifurcation with complex boundary geometries. Alternatively, one can use numerical methods including finite element methods [15] and boundary integral methods [26] to compute Stokes flows in a bifurcation. Considering the

computational costs of domain discretisation and efforts of dealing with corner singularities, however, these methods are too computationally expensive to run thousands of simulations to comprehensively interrogate the parameter space.

Recent developments in rational approximation [4, 5, 11, 22] have underpinned novel algorithms to compute 2D Stokes flows in bifurcations using an applied complex variable approach [3, 37]. In 2019, Gopal and Trefethen [11] introduced the lightning algorithm for solving Laplace's equation in polygon domains using rational functions. The lightning algorithm achieves a root-exponential convergence by clustering poles exponentially near corners, providing an optimal way to deal with corner singularities. Brubeck and Trefethen [3] applied the lightning algorithm to 2D Stokes flow problems. The stream function, that satisfies the biharmonic equation, can be represented using two complex analytic Goursat functions [12] and approximated by rational functions. Based on the lightning algorithm, we have developed the LARS (Lightning-AAA Rational Stokes) algorithm [37] for computing 2D Stokes flows in general domains, including domains which have curved boundaries or are multiply connected. The computation usually takes less than one second on a laptop and gives solutions with at least 6-digit accuracy [37].

In this work, we use the LARS algorithm to compute Stokes flows in 2D bifurcation with different geometrical and flow conditions. For bifurcations with different channel widths, bifurcation angles, boundary geometry, we compute the flux-pressure relationship and compare against Poiseuille's law approximations. We show that the impact of bifurcation geometry on the flux-pressure relationship can be considered accurately using a Y-shaped network, which can be incorporated into a 0D flow network model easily. Furthermore, we present flow features that cannot be captured by a 0D network model, including streamline patterns, flow separation in a bifurcation, and effects of fixed objects on the pressure-flux relationship of a bifurcation.

2 Problem formulation

In a Cartesian coordinate system $\mathbf{x} = (x, y)^T$, we consider a 2D bifurcation with one inlet parent branch with width d, and two outlet child branches with widths d_1 and d_2, respectively. We place the origin at the intersection of the centrelines of the channels. The angle between the positive x axis and the two branch centrelines are denoted α and β, respectively. Each channel has centreline length l.

We consider steady flow of an incompressible Newtonian viscous fluid governed by the Stokes and continuity equations:

$$\mu \nabla^2 \mathbf{u} = \nabla p, \ \nabla \cdot \mathbf{u} = 0, \tag{2}$$

where $\mathbf{u} = (u, v)^T$ is the 2D velocity field, p is the pressure and μ is the viscosity. We prescribe normal stress and parallel flow boundary conditions at inlet and outlets, and zero velocity boundary condition on the walls. The flow is thus assumed to enter and exit the bifurcation region with fully developed parabolic flow.

3

We non-dimensionalise as follows

$$\mathbf{X} = \frac{\mathbf{x}}{d}, \ \mathbf{U} = \frac{\mathbf{u}}{q/d}, P = \frac{p}{\mu q/d^2}, \tag{3}$$

where capitals denote dimensionless variables. The dimensionless Stokes equations in component form, together with the continuity equation, then become

$$\frac{\partial^2 U}{\partial X^2} + \frac{\partial^2 U}{\partial Y^2} = \frac{\partial P}{\partial X}, \tag{4}$$

$$\frac{\partial^2 V}{\partial X^2} + \frac{\partial^2 V}{\partial Y^2} = \frac{\partial P}{\partial Y}, \tag{5}$$

$$\frac{\partial U}{\partial X} + \frac{\partial V}{\partial Y} = 0. \tag{6}$$

We set the dimensionless centreline length $L = l/d = 2$ for each channel to ensure the flow domain has sufficient length that the flow is fully developed at the outlets. We assume the dimensionless pressure at inlet $P_0 = 0$. For a 2D bifurcation, we now have 6 dimensionless parameters: child branch widths D_1 and D_2, outlet pressures P_1 and P_2 and bifurcation angles α and β. Figure 1 shows the dimensionless Stokes flow problem in a 2D bifurcation.
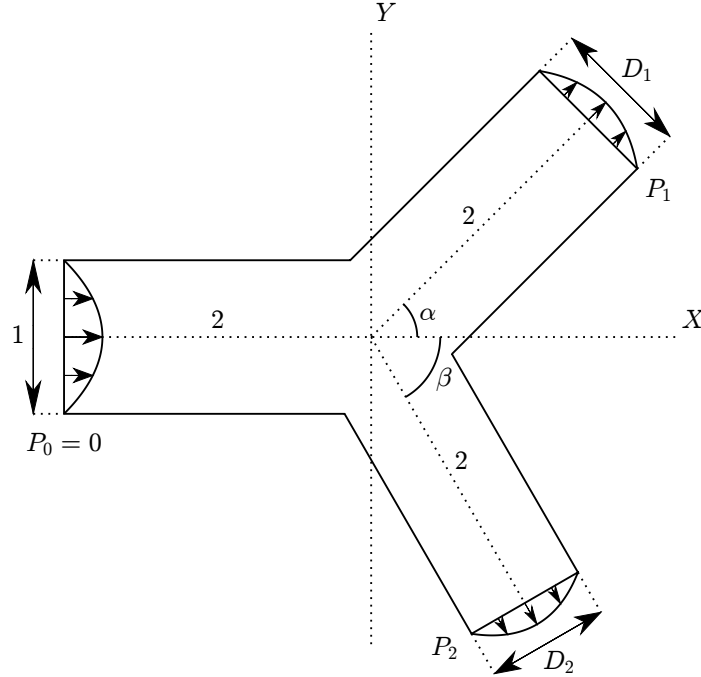

Fig. 1: Schematic of Stokes flows through a 2D bifurcation.

3 Representation of the bifurcation using a flow network model

The pressure-flux relationship of Stokes flows at a bifurcation can be represented using a Y-shaped flow network model as shown in Figure 2. The fluxes in flow segments are Q, Q_1 and Q_2, where the arrows indicate the directions in which the flux is positive. For any bifurcation, there are three unknown flow conductance G_{0c}, G_{1c} and G_{2c} that depend on the bifurcation geometry.
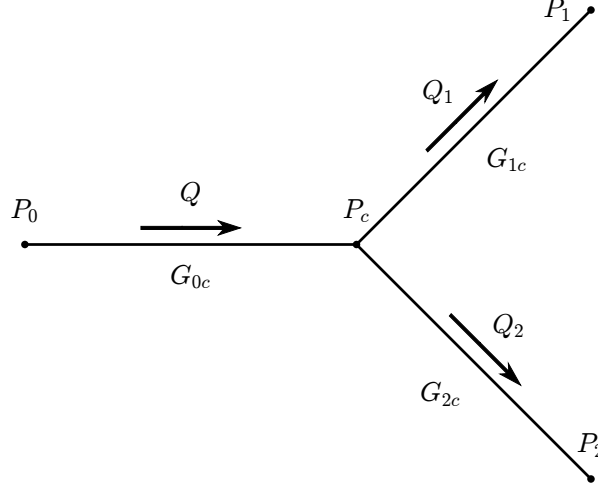

Fig. 2: Schematic of the flow network that represents the bifurcation.

The dimensionless fluxes in flow segments are related via

$$Q = Q_1 + Q_2 = G_{0c}(P_0 - P_c), \ Q_1 = G_{1c}(P_c - P_1), \ Q_2 = G_{2c}(P_c - P_2). \quad (7)$$

When $P_0 = 0$,

$$P_c = \frac{G_{1c}P_1 + G_{2c}P_2}{G_{0c} + G_{1c} + G_{2c}}. \quad (8)$$

From (7), we now have a linear system relating the pressures and fluxes at two outlets:

$$\begin{bmatrix} \dfrac{-G_{1c}G_{2c} - G_{1c}G_{0c}}{G_{0c} + G_{1c} + G_{2c}} & \dfrac{G_{1c}G_{2c}}{G_{0c} + G_{1c} + G_{2c}} \\ \dfrac{G_{1c}G_{2c}}{G_{0c} + G_{1c} + G_{2c}} & \dfrac{-G_{2c}G_{1c} - G_{2c}G_{0c}}{G_{0c} + G_{1c} + G_{2c}} \end{bmatrix} \begin{bmatrix} P_1 \\ P_2 \end{bmatrix} = \begin{bmatrix} Q_1 \\ Q_2 \end{bmatrix}, \quad (9)$$

represented by

$$\mathbf{GP} = \mathbf{Q}. \quad (10)$$

5

When two solutions of flux vector $\mathbf{Q}$ for two linear independent $\mathbf{P}$ (e.g. $\mathbf{P} = [1\ 0]^T$ and $\mathbf{P} = [0\ 1]^T$) are provided, the rank 2 conductance tensor $\mathbf{G}$ and three unknown components G_{0c}, G_{1c} and G_{2c} can be calculated for flux predictions for different pressure conditions. Note that we can only have this linear relationship (10) for Stokes flows, since the Stokes equations are linear.

If the junction is simplified as a node and the fluid flow in each segment is assumed to be fully developed, we can approximate three unknown flow conductance using Poiseuille's law for 2D channel flows [32]:

$$\tilde{G}_{0c} = \frac{1}{12L}, \ \tilde{G}_{1c} = \frac{D_1^3}{12L}, \ \tilde{G}_{2c} = \frac{D_2^3}{12L}, \tag{11}$$

where $\tilde{G}$ is the idealised flow conductance. Using (9) and (11), the pressure-flux relationship for an idealised 2D bifurcation can be approximated by

$$\begin{bmatrix} \dfrac{-D_1^3 D_2^3 - D_1^3}{12L(1 + D_1^3 + D_2^3)} & \dfrac{D_1^3 D_2^3}{12L(1 + D_1^3 + D_2^3)} \\ \dfrac{D_1^3 D_2^3}{12L(1 + D_1^3 + D_2^3)} & \dfrac{-D_1^3 D_2^3 - D_2^3}{12L(1 + D_1^3 + D_2^3)} \end{bmatrix} \mathbf{P} = \tilde{\mathbf{G}}\mathbf{P} = \mathbf{Q}. \tag{12}$$

We refer to this as Poiseuille's law approximation in this paper, to distinguish it from the pressure-flux relationship calculated from Stokes flow simulations.

4 Computing 2D Stokes flows via rational approximation

The Poiseuille's law approach (12) has been widely used to compute fluxes in large flow networks, and usually provided good approximations. In this paper, we aim to compute the pressure-flux relationship for general bifurcations with different geometries by solving the 2D Stokes equations. Using the LARS algorithm [37], which uses an applied complex variable approach with rational approximation, the 2D Stokes flow problems can be computed with great speed and accuracy. In this section, we summarise the LARS algorithm for computing 2D Stokes flows. Further details about the algorithm can be found at [37]

4.1 The Goursat representation for biharmonic equations

We define a stream function ψ for the dimensionless Stokes flow problem as

$$U = \frac{\partial \psi}{\partial Y}, \ V = -\frac{\partial \psi}{\partial X}, \tag{13}$$

which satisfies the biharmonic equation

$$\nabla^4 \psi = 0. \tag{14}$$

6

In the complex plane $\zeta = X + iY$, where $i = \sqrt{-1}$, we have

$$\frac{\partial}{\partial \zeta} = \frac{1}{2}\left(\frac{\partial}{\partial X} - i\frac{\partial}{\partial Y}\right), \ \frac{\partial}{\partial \bar{\zeta}} = \frac{1}{2}\left(\frac{\partial}{\partial X} + i\frac{\partial}{\partial Y}\right), \tag{15}$$

where overbars denote complex conjugates. Then the biharmonic equation can be rewritten as

$$\frac{\partial^4 \psi}{\partial^2 \zeta \partial^2 \bar{\zeta}} = 0, \tag{16}$$

which has a solution in the form

$$\psi(\zeta, \bar{\zeta}) = \text{Im}[\bar{\zeta} f(\zeta) + g(\zeta)], \tag{17}$$

where $f(\zeta)$ and $g(\zeta)$ are two analytic functions in the fluid domain, known as the Goursat functions [12]. The dimensionless velocity, pressure and vorticity magnitude ($\Omega = \partial V/\partial X - \partial U/\partial Y$) can then be expressed in terms of Goursat functions as

$$U - iV = -\overline{f(\zeta)} + \bar{\zeta} f'(\zeta) + g'(\zeta), \tag{18}$$

$$P - i\Omega = 4f'(\zeta). \tag{19}$$

The Goursat representation satisfies the biharmonic equation by construction. To solve the Stokes flow problem, we therefore need to determine the Goursat functions such that the boundary conditions are satisfied.

4.2 Approximating the Goursat functions using rational functions

The LARS algorithm approximates the Goursat functions using rational functions [37]. The rational function bases have clustering poles towards sharp corners [3, 11] and near smooth boundaries [5, 22], Laurent series for multiply connected domains [27, 34], and a polynomial for remaining smooth part of the solution. This leads to a rational function $r(\zeta)$ in the form:

$$r(\zeta) = \sum_{j=1}^{m} \frac{a_j}{\zeta - z_j} + \sum_{j=0}^{n} b_j \zeta^j + \sum_{i=1}^{p}\sum_{j=1}^{q} c_{ij}(\zeta - \zeta_i)^{-j}, \tag{20}$$

where a, b and c are complex coefficients to be determined, z are poles and ζ_i is a point in the ith hole. Note that we also need to include two log terms in two Goursat functions (one for $f(\zeta)$ and one for $g(\zeta)$) corresponding to each hole, due to the logarithmic conjugation theorem [2, 27].

It has been shown that an analytic function in a polygon domain can be approximated with a root-exponential convergence, if the poles are exponentially clustered near corner singularities [11]. This leads to the lightning algorithm for computing Laplace problems [11] and 2D Stokes flows [3] in polygon domains. For bifurcations with sharp corners, we follow the lightning algorithm to place poles clustering towards each corner singularity.

For bifurcations with smooth boundaries, we first approximate the Schwarz function $F(\zeta) = \bar{\zeta}$ on each curved boundary using the AAA algorithm [5, 22]. The AAA algorithm searches for the best rational approximation in a barycentric form automatically. We choose the Schwarz function here, because it only depends on the boundary shape instead of the boundary value. After finding the rational function that approximates the boundary shape, we use its poles outside the domain to approximate the Goursat functions. This is known as the AAA-least squares approximation [5].

We perform a Vandermonde with Arnoldi orthogonalization [4] to construct a well-conditioned basis for the polynomial, poles and Laurent series. Imposing the boundary conditions of the fluid problem (18, 19), the complex coefficients a, b and c in two Goursat functions can be computed easily by solving a least-squares problem. The computation is carried out using MATLAB and example codes are available in [3, 37].

5 Results

Using the LARS algorithm, we present Stokes flows in 2D bifurcations with different geometries including child branch widths, bifurcation angles and boundary geometries. We also consider bifurcations with obstacles inside (e.g. a cylinder) and quantify their impact on the pressure-flux relationship. We will compute the conductance tensor $\mathbf{G}$ (9) for different bifurcation geometries, and compare these against the Poiseuille's law approximation (12) where applicable.

5.1 2D Stokes flows in a bifurcation

Figure 3 presents the Stokes flows in a typical 2D bifurcation computed by the lightning algorithm [3], where $D_1 = 0.9$, $D_2 = 0.8$, $\alpha = \pi/4$, $\beta = \pi/3$ and $L = 2$ for $P_1 = P_2 = 0$ and $Q = 1$. We set $P_1 = P_2 = -30$ so that the maximum velocity magnitude is at the order of 1. The lightning algorithm places poles exponentially clustered towards three sharp corners of the geometry, where the placement of poles are indicated by red dots in Figure 3. Using a polynomial of degree 24 with 48 poles clustered near each corner, a solution can be computed in less than one second on an Apple laptop with an M1 chip. The maximum error in dimensionless velocity components and pressures on the domain boundary is less than 10^{-6}.

5.2 Effects of channel width on the flow network representation

For a bifurcation consisting of 3 straight channels with $L = 2$, the geometry has four degrees of freedom: D_1, D_2, α and β. To investigate the effects of the width of two child branches, we set the bifurcation angles $\alpha = \pi/4$ and $\beta = \pi/4$, and investigate the effects of changing the bifurcation angles in Section 5.3. Figure 4 shows the relative differences in G_{0c}, G_{1c} and G_{2c} from 2D Stokes flows simulations, compared with Poiseuille's law approximations for $D_1, D_2 \in [0.5, 1]$. For each combination of D_1 and D_2, we perform two Stokes flow simulations for two outlet pressure conditions, and compute the three flow conductance using Eq. 9. The black curve indicates the possible widths of two child branches, if they obey Murray's law [21] in 2D: $D_1^2 + D_2^2 = D^2 = 1$.
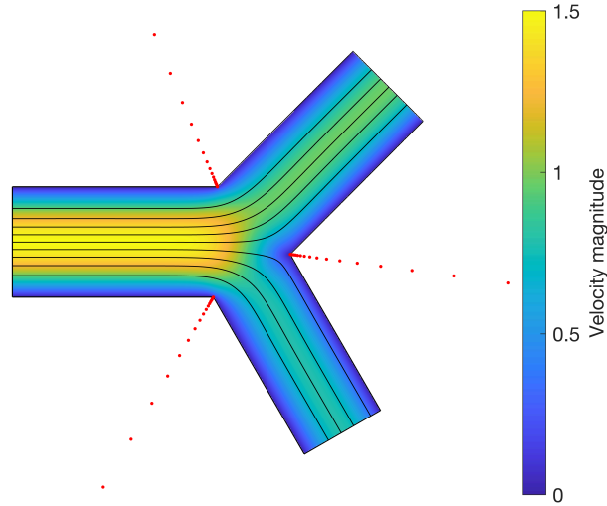
Fig. 3: Stokes flows in a 2D bifurcation for $P_1 = P_2 = 0$ and $Q = 1$, solved by the lightning algorithm, where $D_1 = 0.9$, $D_2 = 0.8$, $\alpha = \pi/4$, $\beta = \pi/3$ and $L = 2$ (same as the bifurcation shown in Figure 1). The streamlines are denoted by black lines and the velocity magnitude is represented by a colourmap. The locations of the poles are marked by red dots.

Note that every term is to the third power in the original Murray's law for 3D problems [21].
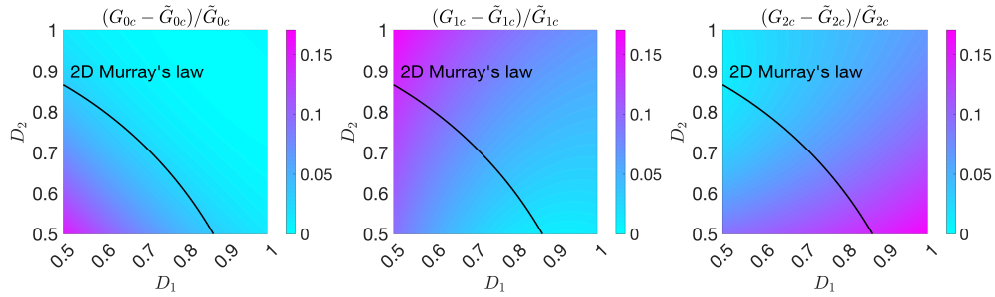

Fig. 4: Relative differences in G_{0c}, G_{1c} and G_{2c} from 2D Stokes flows simulations, compared with Poiseuille's law approximations for $D_1, D_2 \in [0.5, 1]$, when $\alpha = \pi/4$, $\beta = \pi/4$ and $L = 2$. The black curve indicates the possible widths of two child branches based on Murray's law in 2D.

9

In this parameter space, the conductance approximation based on Poiseuille's law underestimates the flow conductance in two child branches. The error in the flow conductance in the parent branch only becomes significant when D_1 and D_2 are close to 0.5. Furthermore, $(G_{1c} - \tilde{G}_{1c})/\tilde{G}_{1c}$ is up to 16.6%, while $(G_{2c} - \tilde{G}_{2c})/\tilde{G}_{2c}$ is only about 1%, when $D_1 = 0.5$ and $D_2 = 1$. This indicates that the Poiseuille's law approximation underestimates not only the total flux through a bifurcation, but also the fraction of flux that enters the first branch, when $D_1 = 0.5$ and $D_2 = 1$. Similar effects are found in the second branch, when $D_1 = 1$ and $D_2 = 0.5$. Note that these numbers are for $L = 2$. For bifurcations with larger channel lengths, the mismatch between two approximations will be reduced, since Poiseuille's law becomes a more accurate approximation for the conductance of fully developed flows in straight channels.

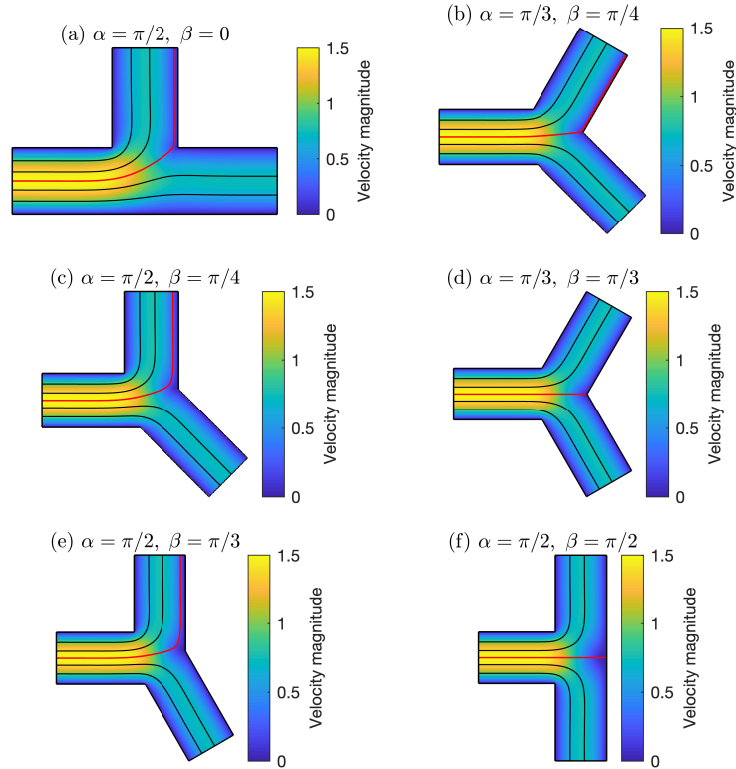## 5.3 Effects of bifurcation angle on flow partition

Fig. 5: Stokes flows in a 2D bifurcation with different bifurcation angles, when $D_1 = D_2 = 1$, $P_1 = P_2 = 0$ and $L = 2$. The centre streamline of the parent branch is coloured in red. Other streamlines are coloured in black.

Figure 5 presents Stokes flows in bifurcations with different bifurcation angles, when $D_1 = D_2 = 1$, $P_1 = P_2 = 0$, $L = 2$ and $Q = 1$. Based on the Poiseuille's law approximation, two child branches should have an even flow partition for all 6 cases. However, Stokes flow simulations reveal that the first branch receives more flow than the second branch in cases (a), (b), (c) and (e). One can observe that the centre streamline of the parent branch (coloured in red), which represents the equal flow partition, enters the first branch in these cases.
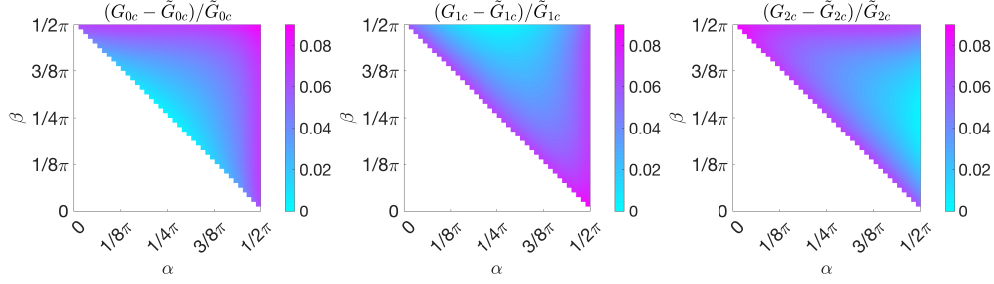

Fig. 6: Relative differences in G_{0c}, G_{1c} and G_{2c} from 2D Stokes flows simulations, compared with Poiseuille's law approximations for different bifurcation angles, when $D_1 = D_2 = 1$ and $L = 2$.

While setting $D_1 = D_2 = 1$ and $L = 2$, we perform a parameter sweep for $\alpha, \beta \in [0, \pi/2]$ except when $|\alpha + \beta| < \pi/2$, since this will lead to a small angle or an overlap between the two child branches. As shown in Figure 6, the Poiseuille's law underestimates the flow conductance in three flow segments, while the maximum errors in G_{0c}, G_{1c} and G_{2c} happen at $\alpha = \beta = \pi/2$; $\alpha = \pi/2$ and $\beta = 0$; and $\alpha = 0$ and $\beta = \pi/2$, respectively. When $\alpha = \pi/2$ and $\beta = 0$, the actual flow conductance in the first branch is about 9% higher than the Poiseuille's law approximation, where the differences in the other two branches are much smaller. This leads to more flow in the first branch than the second branch as shown in cases (a), (c) and (e) in Figure 5, where $\alpha = \pi/2$ and $\beta < \pi/2$.

5.4 Separation of Stokes flows in a 2D bifurcation for different outlet pressures

All pressure-flux relationships in previous examples can be computed using both Stokes flow simulations and Poiseuille's law. We now investigate more complex scenarios that can only be understood using 2D Stokes flow solvers rather than a linear network approach.

The separation of Stokes flows has been studied [6, 18, 20]. In the context of flows in a bifurcation, a similar concept of the separation of microparticle trajectories has been used for studying microparticle advection and partition [1, 7, 35]. Here we

investigate the separation streamline (i.e. the streamline that separates the flows into two branches) of 2D Stokes flows in a bifurcation for different P_1 and P_2.

In this section, we set $D_1 = D_2 = 1$, $\alpha = \beta = \pi/4$ and $L = 2$ for the bifurcation geometry. We set the inlet flux $Q = 1$ rather than inlet pressure P_0, so the flow now is only dependent on outlet pressure difference $P_1 - P_2$. Figure 7 displays the streamlines that separate the flows for different $P_1 - P_2$. For cases (a)-(c), the red streamline separates the flow that enters two child branches. For cases (d)-(f), the red streamline separates the flow from the parent branch and the first branch that enters the second branch, since the flow direction reverses in the first branch. Based on Stokes flow simulations, the reverse flow appears when $P_1 - P_2 > 22.49$, while it is estimated to be $P_1 - P_2 = 24$ using Poiseuille's law.
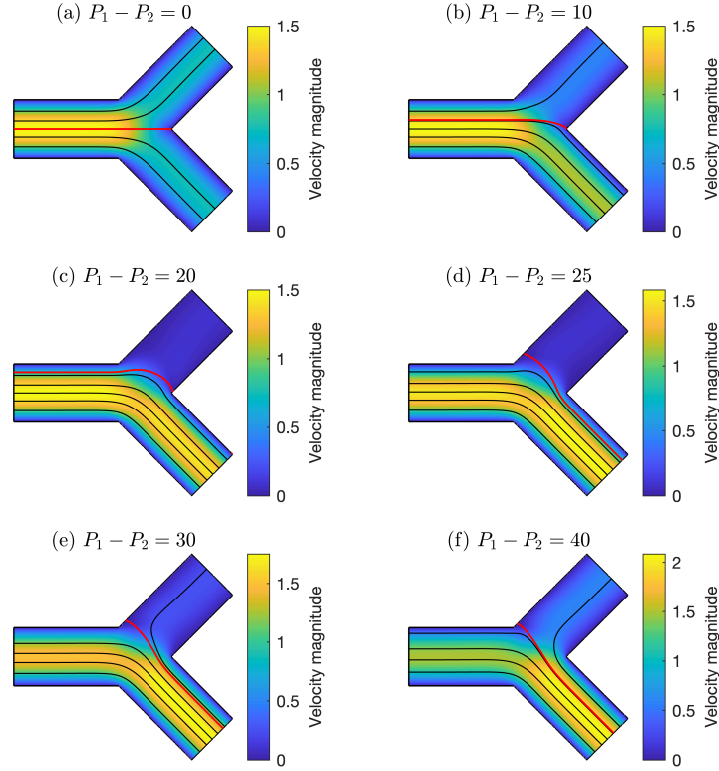

Fig. 7: Stokes flows in a 2D bifurcation for different $P_1 = P_2$, when $D_1 = D_2 = 1$, $\alpha = \beta = \pi/4$, $L = 2$ and $Q = 1$. The streamline that separates the flows into (or from) two branches is coloured in red. Other streamlines are coloured in black.

5.5 Effects of boundary geometry on bifurcation flow

We now study the flow partition in bifurcations with curved boundaries. We replace the boundary walls with cubic Bézier curves with two control points at two ends and the other two control points at the location of the original sharp corner. We will show that the flux-pressure relationship in these bifurcation can be represented accurately by a Y-shaped flow network using Stokes flow simulations, due to the linearity of the Stokes equations (2).

Figure 8 presents the Stokes flows computed in the same bifurcation as shown in Figure 1, but with curved boundaries. We use a polynomial of degree 48 with poles placed by the AAA algorithm [5, 22] near the three curved boundaries. The number of AAA poles is much smaller than the lightning poles for sharp corner cases, so we increase the polynomial degree to achieve the same order of accuracy $\mathcal{O}(10^{-6})$.
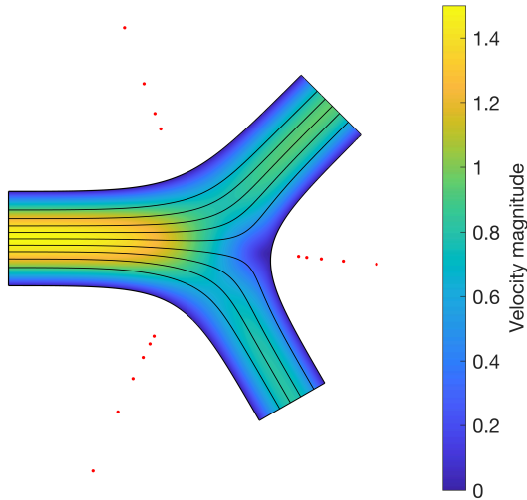

Fig. 8: Stokes flows in a 2D bifurcation with smooth boundaries solved by the LARS algorithm, where $D_1 = 0.9$, $D_2 = 0.8$, $\alpha = \pi/4$, $\beta = \pi/3$, $L = 2$, $P_1 = P_2 = 0$ and $Q = 1$ (same as the bifurcation shown in Figure 1). The streamlines are denoted by black lines and the velocity magnitude is represented by a colourmap. The AAA poles are marked by red dots.

The flow conductance calculated from Stokes flow simulations are $G_{0c} = 0.0509$, $G_{1c} = 0.0403$ and $G_{2c} = 0.0306$, while these are 0.0422, 0.0313 and 0.0226 for the bifurcation consisting of straight channels (while Poiseuille's law gives 0.0417, 0.0304 and 0.0213). The increase of flow conductance in each segment is due to the increase in the bifurcation area. The large differences between these two geometries demonstrate the needs of updating the conductance components of the flow network based on

13

detailed flow simulations for representing the accurate flux-pressure relationship at a bifurcation.

We can now use the computed flow conductance components and (9) to construct an updated Y-shaped flow network to predict the flow partition at the bifurcation (Figure 8) for different outlet pressures. The maximum relative difference in Q_1 for $P_1, P_2 \in [-20, 20]$ between the updated flow network predictions and Stokes flow simulations is $\mathcal{O}(10^{-10})$, several orders of magnitude below the numerical accuracy of these simulations: $\mathcal{O}(10^{-6})$. This shows that the flux-pressure relationship of Stokes flows in a bifurcation with any shape can be simply represented using a Y-shaped flow network, given that the flow is fully developed entering and exiting the domain.

5.6 Effects of fixed objects on bifurcation flow

As already seen, a Y-shaped flow network is a valid approximation for pressure-flux relationship for a range of conditions of Stokes flows in a 2D bifurcation. We now consider multiply connected problems of bifurcations containing fixed objects. We consider a simple case with only one fixed cylinder in a symmetrical bifurcation ($D_1 = D_2 = 1$, $\alpha = \beta = \pi/4$ and $L = 2$) to investigate the effects of the location and size of the cylinder on the three flow conductance components. The cylinder has a centre coordinate (X_0, Y_0) and a radius R.
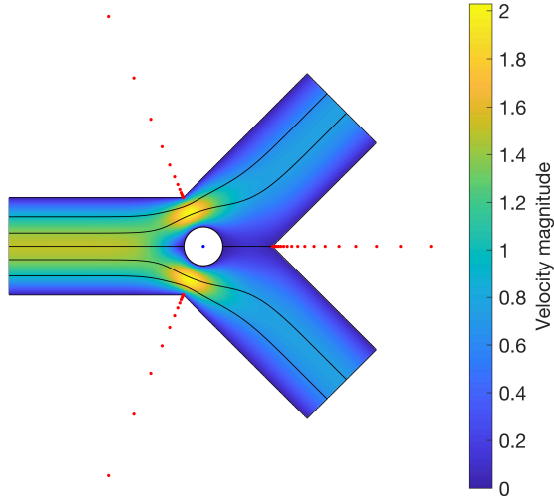

Fig. 9: Stokes flows in a 2D bifurcation with a fixed cylinder at $(X_0, Y_0) = (0, 0)$ and $R = 0.2$ solved by the LARS algorithm, where $D_1 = D_2 = 1$, $\alpha = \beta = \pi/4$, $L = 2$, $P_1 = P_2 = 0$ and $Q = 1$. The locations of the poles and Laurent series are marked by red and blue dots, respectively.

14

Figure 9 shows the Stokes flows computed in a bifurcation for $D_1 = D_2 = 1$, $\alpha = \beta = \pi/4$, $L = 2$, $P_1 = P_2 = 0$ and $Q = 1$, with a fixed cylinder with $(X_0, Y_0) = (0, 0)$ and $R = 0.2$. In addition to poles and a degree 80 polynomial, we also include a degree 20 Laurent series about the centre of the cylinder (blue points) in the rational function basis, as shown in Figure 8. The solution is computed to the accuracy $\mathcal{O}(10^{-5})$ in 1.5 seconds. A similar case has been considered in [37], where one can find further details of the numerical algorithm.

For this complex geometry, one can also find a network representation for the pressure-flux relationship between the three openings (9). Figure 10 shows the effects of (X_0, Y_0) and R on the flow conductance of three channels. The presence of a fixed cylinder mainly reduces the flow conductance (or increases the flow resistance) of the segment containing the cylinder, while slightly affects other segments, as represented by the cyan regions in Figure 10. This local effect suggests that only updating the flow conductance of the segment containing the cylinder may give a good approximation for the pressure-flux relationship of a bifurcation and even a flow network which consists of a large number of bifurcations. Its potential application to network flows will be discussed in the next section.
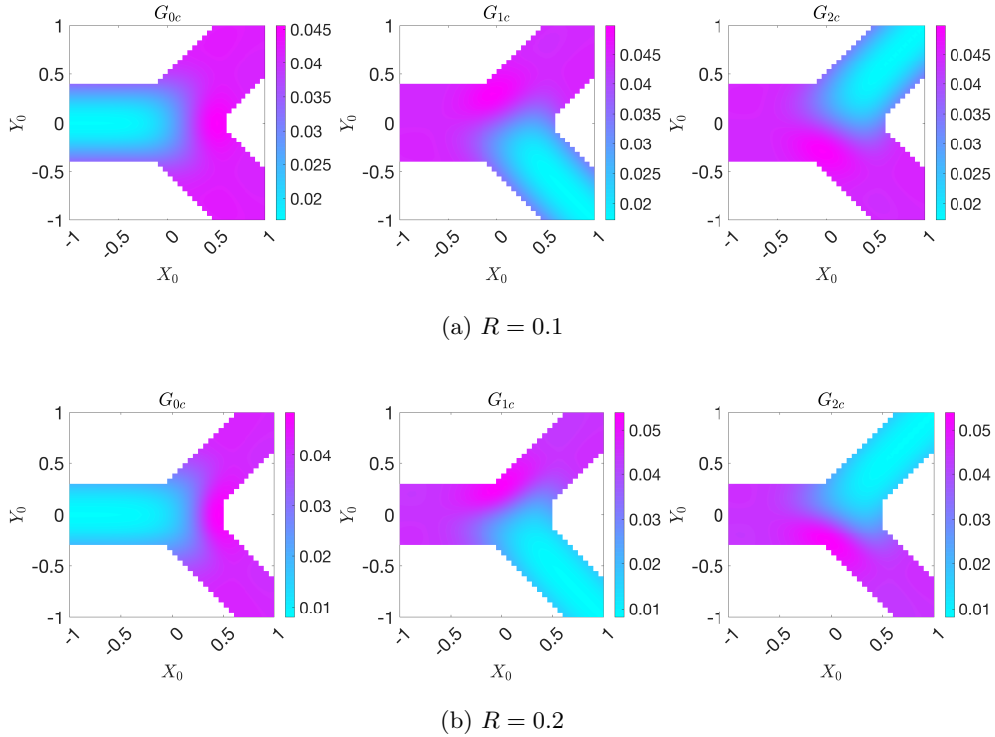

(a) $R = 0.1$

(b) $R = 0.2$

Fig. 10: G_{0c}, G_{1c} and G_{2c} of a bifurcation with $D_1 = D_2 = 1$, $\alpha = \beta = \pi/4$ and $L = 2$, when there is a fixed cylinder with different centre location (X_0, Y_0) and radius R.

15

We also consider the impact of cylinder sizes on flow conductance, where $R = 0.1$ in Figure 10a and $R = 0.2$ in Figure 10b. When the cylinder radius doubles from 0.1 to 0.2, the flow conductance is halved from 0.02 to 0.01. In addition, the flow conductance is higher when the gap between the cylinder and the channel wall is smaller. This stresses the need of considering the lateral location of the cylinders or other finite sized objects for accurate flow conductance computations. However, the effect of lateral location on flow conductance is less significant for larger cylinders ($R = 0.2$), as the magenta boundaries near the channel walls disappear in Figure 10b.

6 Discussion

In this paper, we computed 2D Stokes flows in a single bifurcation, and investigated the effects of bifurcation geometry on flows, especially the pressure-flux relationship between inlet and outlets. Making full advantage of the great speed and accuracy of our 2D Stokes flow solver [37], we performed simulations for parameters including child branch widths and bifurcation angles. In addition, we investigated the separation of Stokes flows in a bifurcation for different outlet pressures. We considered the effects of domain boundaries and fixed objects on Stokes flows in a bifurcation.

Our simulation results show that the bifurcation geometry can have an impact on Stokes flows for a given boundary condition. Even when only interested in the pressure-flux relationship, the geometrical effects cannot be fully captured by the 0D Poiseuille's law model. In section 5.3, we present Stokes flows in bifurcations with the same channel widths, but different branching angles. All these bifurcations are represented by the same flow network model, if the flow conductance components are approximated by Poiseuille's law. However, the Poiseuille's law approximation of flow conductance can have an error up to 9% for $L = 2$ in the parameter space of α and β in Figure 6.

In this paper, we assume $L = 2$ across all simulations. For a larger L, the flow will have a parabolic-like profile in a larger fraction of a channel where the Poiseuille's law provides a very good approximation, so the error in flow conductance will be reduced. Conversely, for a smaller L, Poiseuille's law approximation may become less accurate. For a much smaller L, it is possible that even the boundary conditions set in our 2D Stokes flow simulations may no longer accurately represent the underlying physics.

Since the Stokes equations are linear, the solutions of any physical quantity should be able to add linearly to construct a new solution, when their boundary conditions are added up. Here we only exploit the linearity between fluxes and pressure boundary conditions for different bifurcation geometries, to provide the foundation for a more systemic workflow that will enable precise reduced-order modelling of flows and particles in a complex network.

We have shown that the pressure-flux relationship of 2D Stokes flows in a bifurcation of any geometry can be represented by an updated 0D flow network based on 2D flow simulation results. The flow conductance tensor in the updated network model only depend on bifurcation geometry, and it can predict fluxes for any pressure boundary conditions.

In a flow network that consists of several orders of bifurcations with known boundary pressure conditions, the maximum flux error in Poiseuille's law approximation is expected to be larger than that in a single bifurcation model. At a bifurcation, the errors are usually not symmetric between two child branches (e.g. see Figure 6), resulting in an inaccurate prediction of flow partition with errors that can be accumulated over bifurcations of different orders. This suggests that replacing each bifurcation node in a flow network with a Y-shaped network that considers the bifurcation geometry may significantly improve the pressure-flux calculation. However, the improvements and associated increase in computational cost require investigation in future work.

We have also considered fixed objects in a bifurcation and their impact on the pressure-flux relationship. Our results show that the object mainly reduces the flow conductance of the channel containing the object, while having little effect on other segments. This local effect holds even when the object centre is within one channel width from the bifurcation centre (Figure 10). For computing the pressure-flux relationship of a large 2D flow network with multiple objects, we may identify segments with object, and only update the flow conductance of these segments considering local objects. The update will be based on 2D Stokes flow simulations [37], or a machine learning model that learns from high-fidelity simulation results [9]. Similar local effects are expected for 3D flows and moving objects, but these require future work.

It should be noted that the updated network model, despite considering bifurcation geometries in pressure-flux relationship, is still a 0D approach that compresses most flow information. The flow details can be extremely useful when considering advective transport of finite size objects [1] or advection-diffusion of tiny particles [38], and these can only be obtained by Stokes flow simulations [37]. One example shown here in Section 5.6 reveals that the flow conductance tensor of a bifurcation (or even a channel) with a fixed cylinder depends on the lateral location of the cylinder, a result that cannot be obtained from a 0D model.

All results presented in this work are purely 2D, but these can provide insight on 3D network flow problems. A similar Y-shaped flow network for the pressure-flux relationship can be derived for any 3D bifurcation from 3D Stokes flow simulations, since 3D Stokes equations are still linear. However, the parameter space that defines a 3D bifurcation is expected to be larger, leading to a more complex problem to be considered comprehensively. For example, the centreline of three branches are not necessarily in the same plane. A future work on 3D bifurcations is thus necessary before translating the findings from this paper to 3D scenarios.

Lastly, all results presented in this work are based on numerical simulations. The simulation results require validation against fluid dynamics experiments in future studies. Such experiments can be carried out in bifurcating flow chambers with sufficient height to mimic infinite channel walls. Then the 2D fluid velocity can be measured on a horizontal cut of the chamber using a particle imaging velocimetry [36].

17

References

[1] Audet D, Olbricht W (1987) The motion of model cells at capillary bifurcations. Microvasc Res 33(3):377–396. https://doi.org/10.1016/0026-2862(87)90029-X

[2] Axler S (1986) Harmonic functions from a complex analysis viewpoint. Amer Math Monthly 93(4):246–258. https://doi.org/10.2307/2323672

[3] Brubeck PD, Trefethen LN (2022) Lightning Stokes solver. SIAM J Sci Comput 44(3):A1205–A1226. https://doi.org/10.1137/21M1408579

[4] Brubeck PD, Nakatsukasa Y, Trefethen LN (2021) Vandermonde with Arnoldi. SIAM Rev 63(2):405–415. https://doi.org/10.1137/19M130100X

[5] Costa S, Trefethen LN (2021) AAA-least squares rational approximation and solution of Laplace problems. arXiv preprint arXiv:210701574 https://doi.org/10.48550/arXiv.2107.01574

[6] Dean WR, Montagnon PE (1949) On the steady motion of viscous liquid in a corner. Math Proc Camb Philos Soc 45(3):389–394. https://doi.org/10.1017/S0305004100025019

[7] Doyeux V, Podgorski T, Peponas S, et al (2011) Spheres in the vicinity of a bifurcation: elucidating the Zweifach–Fung effect. J Fluid Mech 674:359–388. https://doi.org/10.1017/S0022112010006567

[8] d'Esposito A, Sweeney PW, Ali M, et al (2018) Computational fluid dynamics with imaging of cleared tissue and of in vivo perfusion predicts drug uptake and treatment responses in tumours. Nat Biomed Eng 2(10):773–787. https://doi.org/10.1038/s41551-018-0306-y

[9] Ebrahimi S, Bagchi P (2022) Application of machine learning in predicting blood flow and red cell distribution in capillary vessel networks. J R Soc Interface 19(193):20220306. https://doi.org/10.1098/rsif.2022.0306

[10] Fung YC (2013) Biomechanics: Circulation, 2nd edn. Springer

[11] Gopal A, Trefethen LN (2019) Solving Laplace problems with corner singularities via rational functions. SIAM J Numer Anal 57(5):2074–2094. https://doi.org/10.1137/19M125947X

[12] Goursat E (1898) Sur l'équation $\Delta\Delta u = 0$. Bull Soc Math France 26:236–237

[13] Hartung G, Badr S, Moeini M, et al (2021) Voxelized simulation of cerebral oxygen perfusion elucidates hypoxia in aged mouse cortex. PLoS Comput Biol 17(1):e1008584. https://doi.org/10.1371/journal.pcbi.1008584

[14] Jeong JT (2001) Slow viscous flow in a partitioned channel. Phys Fluids 13(6):1577–1582. https://doi.org/10.1063/1.1367324

[15] Logg A, Mardal KA, Wells G (2012) Automated solution of differential equations by the finite element method: The FEniCS book. Springer

[16] Luca E, Llewellyn Smith SG (2018) Stokes flow through a two-dimensional channel with a linear expansion. Q J Mech Appl Math 71(4):441–462. https://doi.org/10.1093/qjmam/hby013

[17] Merlo A, Berg M, Duru P, et al (2022) A few upstream bifurcations drive the spatial distribution of red blood cells in model microfluidic networks. Soft Matter 18(7):1463–1478. https://doi.org/10.1039/D1SM01141C

[18] Michael D, O'Neill M (1977) The separation of Stokes flows. J Fluid Mech 80(4):785–794. https://doi.org/10.1017/S0022112077002481

[19] Miller C, Padmos RM, van der Kolk M, et al (2021) In silico trials for treatment of acute ischemic stroke: Design and implementation. Comput Biol Med 137:104802. https://doi.org/10.1016/j.compbiomed.2021.104802

[20] Moffatt HK (1964) Viscous and resistive eddies near a sharp corner. J Fluid Mech 18(1):1–18. https://doi.org/10.1017/S0022112064000015

[21] Murray CD (1926) The physiological principle of minimum work: I. the vascular system and the cost of blood volume. Proc Natl Acad Sci USA 12(3):207–214. https://doi.org/10.1073/pnas.12.3.207

[22] Nakatsukasa Y, Sète O, Trefethen LN (2018) The AAA algorithm for rational approximation. SIAM J Sci Comput 40(3):A1494–A1522. https://doi.org/10.1137/16M1106122

[23] Oh KW, Lee K, Ahn B, et al (2012) Design of pressure-driven microfluidic networks using electric circuit analogy. Lab Chip 12(3):515–545. https://doi.org/10.1039/c2lc20799k

[24] Padmos RM, Józsa TI, El-Bouri WK, et al (2021) Coupling one-dimensional arterial blood flow to three-dimensional tissue perfusion models for in silico trials of acute ischaemic stroke. Interface focus 11(1):20190125. https://doi.org/10.1098/rsfs.2019.0125

[25] Pop S, Richardson G, Waters S, et al (2007) Shock formation and non-linear dispersion in a microvascular capillary network. Math Med Biol 24(4):379–400. https://doi.org/10.1093/imammb/dqm007

[26] Pozrikidis C (1992) Boundary integral and singularity methods for linearized viscous flow. Cambridge University Press

[27] Price T, Mullin T, Kobine J (2003) Numerical and experimental characterization of a family of two-roll-mill flows. Proc R Soc A 459(2029):117–135. https://doi.org/10.1098/rspa.2002.1022

[28] Pries AR, Neuhaus D, Gaehtgens P (1992) Blood viscosity in tube flow: dependence on diameter and hematocrit. Am J Physiol 263(6):H1770–H1778. https://doi.org/10.1152/ajpheart.1992.263.6.H1770

[29] Secomb TW (2017) Blood flow in the microcirculation. Annu Rev Fluid Mech 49:443–461. https://doi.org/10.1146/annurev-fluid-010816-060302

[30] Secomb TW, Hsu R, Park EY, et al (2004) Green's function methods for analysis of oxygen delivery to tissue by microvascular networks. Ann Biomed Eng 32:1519–1529. https://doi.org/10.1114/B:ABME.0000049036.08817.44

[31] Su SW, Catherall M, Payne S (2012) The influence of network structure on the transport of blood in the human cerebral microvasculature. Microcirculation 19(2):175–187. https://doi.org/10.1111/j.1549-8719.2011.00148.x

[32] Sutera SP, Skalak R (1993) The history of Poiseuille's law. Annu Rev Fluid Mech 25(1):1–20. https://doi.org/10.1146/annurev.fl.25.010193.000245

[33] Tavakol B, Froehlicher G, Holmes DP, et al (2017) Extended lubrication theory: improved estimates of flow in channels with variable geometry. Proc R Soc A 473(2206):20170234. https://doi.org/10.1098/rspa.2017.0234

[34] Trefethen LN (2018) Series solution of Laplace problems. ANZIAM J 60(1):1–26. https://doi.org/10.1017/S1446181118000093

[35] Wang Z, Sui Y, Salsac AV, et al (2018) Path selection of a spherical capsule in a microfluidic branched channel: Towards the design of an enrichment device. J Fluid Mech 849:136–162. https://doi.org/10.1017/jfm.2018.414

[36] Williams J, Castrejon-Pita A, Turney B, et al (2020) Cavity flow characteristics and applications to kidney stone removal. J Fluid Mech 902:A16. https://doi.org/10.1017/jfm.2020.583

[37] Xue Y, Waters SL, Trefethen LN (2023) Computation of 2D Stokes flows via lightning and AAA rational approximation. arXiv preprint arXiv:230613545 https://doi.org/10.48550/arXiv.2306.13545

[38] Yeo E, Markides H, Schade A, et al (2021) Experimental and mathematical modelling of magnetically labelled mesenchymal stromal cell delivery. J R Soc Interface 18(175):20200558. https://doi.org/10.1098/rsif.2020.0558